University of Groningen

Intrinsically unidirectional chemically fuelled rotary molecular motors

Mo, Ke; Zhang, Yu; Dong, Zheng; Yang, Yuhang; Ma, Xiaoqiang; Feringa, Ben L.; Zhao, Depeng

IMPORTANT NOTE: You are advised to consult the publisher's version (publisher's PDF) if you wish to cite from it. Please check the document version below.

Document Version
Publisher's PDF, also known as Version of record

Publication date:
2022

[Link to publication in University of Groningen/UMCG research database](#)

Article

Intrinsically unidirectional chemically fuelled rotary molecular motors

Ke Mo[1,4], Yu Zhang[1,4], Zheng Dong[1], Yuhang Yang[1], Xiaoqiang Ma[1], Ben L. Feringa[2,3 ✉] & Depeng Zhao[1 ✉]

Biological systems mainly utilize chemical energy to fuel autonomous molecular motors, enabling the system to be driven out of equilibrium[1]. Taking inspiration from rotary motors such as the bacterial flagellar motor[2] and adenosine triphosphate synthase[3], and building on the success of light-powered unidirectional rotary molecular motors[4–6], scientists have pursued the design of synthetic molecular motors solely driven by chemical energy[7–13]. However, designing artificial rotary molecular motors operating autonomously using a chemical fuel and simultaneously featuring the intrinsic structural design elements to allow full 360° unidirectional rotary motion like adenosine triphosphate synthase remains challenging. Here we show that a homochiral biaryl **Motor-3**, with three distinct stereochemical elements, is a rotary motor that undergoes repetitive and unidirectional 360° rotation of the two aryl groups around a single-bond axle driven by a chemical fuel. It undergoes sequential ester cyclization, helix inversion and ring opening, and up to 99% unidirectionality is realized over the autonomous rotary cycle. The molecular rotary motor can be operated in two modes: synchronized motion with pulses of a chemical fuel and acid–base oscillations; and autonomous motion in the presence of a chemical fuel under slightly basic aqueous conditions. This rotary motor design with intrinsic control over the direction of rotation, simple chemical fuelling for autonomous motion and near-perfect unidirectionality illustrates the potential for future generations of multicomponent machines to perform mechanical functions.

Molecular motors play a pivotal role in living systems, ranging from energy conversion, locomotion and intracellular transport, to signal transduction and vision[14–16]. In recent decades, remarkable progress has been made towards the design and applications of artificial molecular machines to enable mechanical functions such as motors, muscles, transporters or pumps[17–20]. The first light-driven rotary molecular motor based on an overcrowded alkene was reported in 1999 (ref.[21]), and at the same time 120° directional rotation, using a chemical-fuelled triptycene-based molecular ratchet, was demonstrated[22]. Since these pioneering studies, unidirectional rotation has been realized in a number of systems, including light-driven imine motors[23], molecular motors based on an interlocked macrocycle[24], hemithioindigo rotary motors[25] and our chemical-driven unidirectional motors involving rotation about single bonds[26–28]. However, unlike power-stroke systems driven by light energy[29–35], designing continuous and autonomous chemical-driven rotary motors in a unidirectional manner remains highly challenging, not least because the appropriate Gibbs-free-energy change for each state of rotation about a single bond and the activation energy, that is, the kinetics for each chemical step, should be precisely controlled with a single set of reactions. In 2016, an autonomous chemically driven molecular system based on a catenane with biased directionality involving a Brownian ratchet

mechanism was reported[36]. However, suppressing random Brownian motion and designing an ATPase-like (ATP, adenosine triphosphate) autonomous molecular motor with the intrinsic capability of unidirectional rotation around an axle using a chemical fuel remains elusive. Our group designed chemically driven rotary molecular motors based on biaryl structures with formation of a transient bridge between the aryl groups, which facilitates atropisomeric conformational interconversion with high unidirectionality[26–28]; however, these systems require manipulation of protecting groups or sequential chemical steps and could not be operated autonomously. It should be noted that while we were preparing this manuscript, another group reported a related approach featuring an autonomous fuelled directional rotation about a single covalent bond[37]. Towards the design of fully autonomous rotary motors (Fig. 1), we reasoned that both the stereoselective cyclization and ring-opening reactions (bridge formation and cleavage in the biaryl system) to form the dominant kinetic products are essential to design continuously rotary molecular motors avoiding predominant random Brownian motion. The unidirectionality should be intrinsic to the system (like in ATPase) and is governed by the ratio of the rates of sequential reactions involved in clockwise and anticlockwise rotation.

To address these challenges, a family of biaryl molecular motors was designed. The structure and the essential operational features of the

Fig. 1 | Schematic representation of the design and concept of the continuously rotary molecular motor. a, Structure and key features of the molecular motor. Key elements: stator and rotor, a carboxylic acid group and two hydroxyl groups to form the dynamic covalent ester bond, and two adjacent point chiral elements, which are used to control both the energy barrier of inversion and the unidirectionality of the motor. **b**, The potential energy diagram of the dynamic kinetic hydrolysis process in continuous rotation. $\Delta G°$, the energy difference of kinetic product and thermodynamic product; $\Delta G^{\ddagger}$, the energy barrier of inversion; $\Delta G_1^{\ddagger}$, the hydrolysis energy barrier of kinetic product; $\Delta G_2^{\ddagger}$, hydrolysis energy barrier of thermodynamic product; $\Delta\Delta G^{\ddagger}$, the energy barrier difference between hydrolysis of kinetic product and thermodynamic product. **c**, Schematic representation of the continuously clockwise 360° rotary process of the molecular motor fuelled by chemical energy (green, the carboxylic acid group with two chiral centres at the rotor; red and blue, the hydroxyl groups at the stator). The chemical-fuelled cycle starts from the open state, and the carboxylic acid group (green) on the rotor reacts highly selectively with the right hydroxyl group (red) on the stator owing to the two adjacent stereocentres on the side chain (step 1). The high-energy intermediate undergoes relatively quickly helix inversion to the stable state with the rotor part flipping from back to front (step 2). Then the ring is opened by hydrolysis to the non-bridged biaryl state without back flipping (step 3). The remaining half cycle is achieved with the same sequence of steps (steps 4–6). The only difference is that the rotor forms a lactone with the other hydroxyl group (blue) at the stator (step 4) inducing the rotor flipping to the back side (step 5). **d**, Evolution of the structures of molecular motors designed and the ratios of kinetic/thermodynamic (K/T) products after cyclization and helix inversion.

rotary molecular motor (**Motor-3**) are given in Fig. 1a. The clockwise 360° rotary process consists of six steps, including two cyclization steps (step 1 and step 4), two ring inversion steps (step 2 and step 5)

and two ring-opening steps (step 3 and step 6; Fig. 1c). The upper ring (rotor) of the biaryl incorporates a carboxylic acid group at the side chain in the *ortho* position whereas the lower one (stator) adopts two
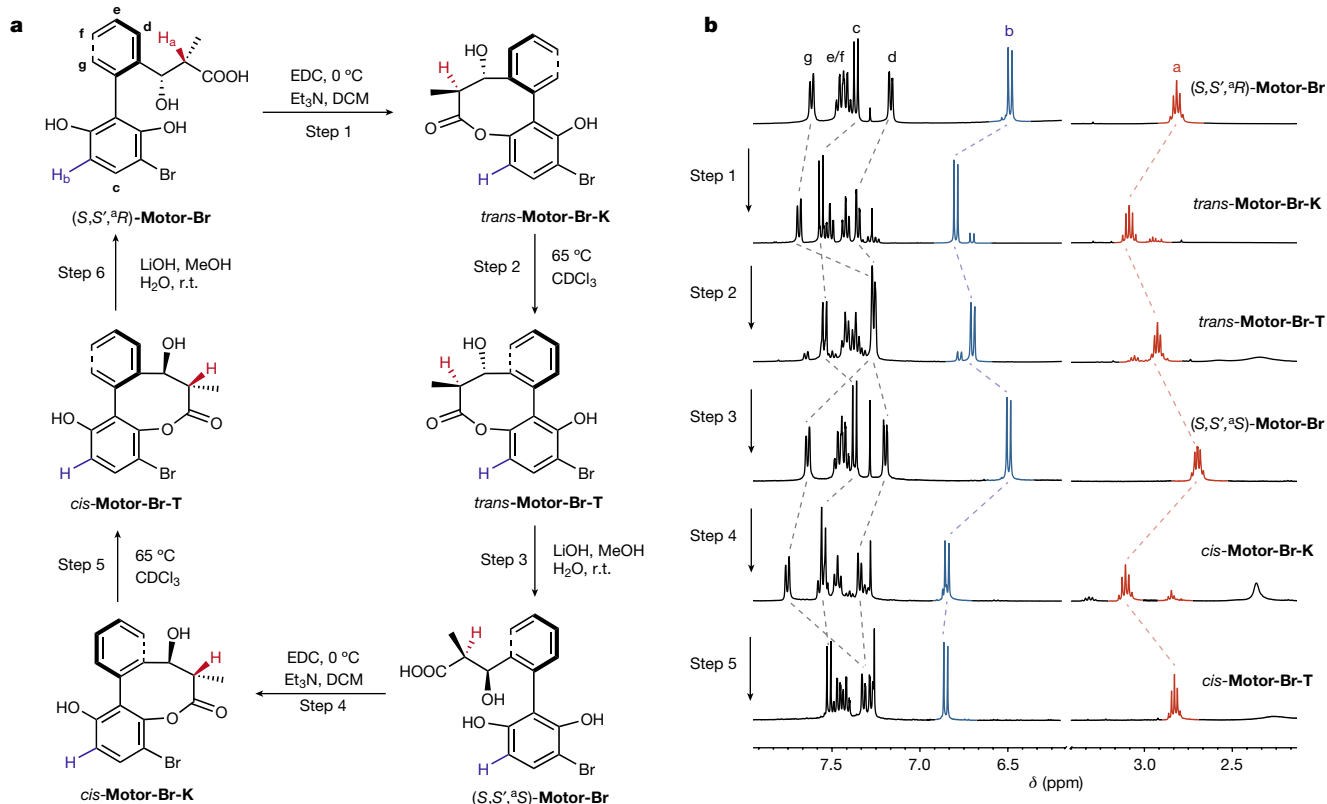
Fig. 2 | Verifying the unidirectional 360° rotation of the molecular motor by desymmetrization of the lower stator. a, Six steps for 360° rotation of the **Motor-Br**. Step 1, EDC, triethylamine (Et$_3$N), DCM, 0 °C, 77%; step 2, 65 °C in CDCl$_3$, quantitative; step 3, LiOH, methanol (MeOH), H$_2$O, room temperature (r.t.), 87%; step 4, EDC, Et$_3$N, DCM, 0 °C, 72%; step 5, 65 °C in CDCl$_3$, quantitative; step 6, LiOH,

MeOH, H$_2$O, r.t., 85%. **b**, Partial ^{1}H NMR spectra of six isomers ((S,S',^aR)-**Motor-Br**, *trans*-**Motor-Br-K**, *trans*-**Motor-Br-T**, (S,S',^aS)-**Motor-Br**, *cis*-**Motor-Br-K** and *cis*-**Motor-Br-T**) in the rotary cycle of the molecular motor (where the superscript 'a' denotes the axial chirality). In steps 1 and 4, the appearance of minor diastereomers is due to helix inversion in the process of isolation. δ.

phenolic groups. The rotation about the sp^2–sp^2 aryl bond is restricted because of the presence of three *ortho* functional groups to avoid random Brownian motion around the single bond without a fuel (Supplementary Fig. 12)[38]. Upon treatment with the fuel, an eight-membered ring lactone is formed and the intramolecular phenolic ester serves as a dynamic covalent bond motif[28]. Each cyclization (steps 1 and 4) is followed by a hydrolysis step (steps 3 and 6) to complete a full rotary cycle (Fig. 1c). The ester formation between the carboxyl group in the rotor aryl and one of the hydroxyl moieties in stator aryl is fuelled by the carbodiimide (*N,N'*-diisopropylcarbodiimide, DIC) to urea (*N,N'*-diisopropylurea, DIU) conversion, which facilitates the biaryl inversion. Key to the design, besides biaryl chirality, are two adjacent stereocentres present in the side chain to control both the cyclization and the inversion processes, respectively. Thus, the point-to-axis chirality induction strategy ensures the unidirectionality of both cyclization and ring-flipping processes.

The second principle used here is dynamic kinetic hydrolysis (steps 2 and 3) of the cyclic states. An ideal potential energy diagram is shown in Fig. 1b. When the molecular motor is operated under strong basic conditions, the selectivity of the ring-opening step is controlled by the ratio of unstable isomer to stable isomer (thermodynamic versus kinetic control), which is determined by the energy difference between two cyclic states ($\Delta G°$). In other words, if $k_{hydrolysis} > k'_{hydrolysis} \gg k_{inversion}$, the ratio of unstable isomer to stable isomer will be the selectivity of the ring-opening step corresponding to unidirectionality in synchronized stepwise motion (Fig. 1c). However, under slightly basic conditions, the hydrolysis speed slows down, and if $k_{inversion} \gg k_{hydrolysis} > k'_{hydrolysis}$, the system follows the Curtin–Hammett principle[39] and the unidirectionality is not solely dependent on the relative proportions of the

interconverting cyclic diastereomers; it is controlled by the difference in energy barrier of the respective transition states $\Delta\Delta G^{\ddagger}$ corresponding to $k_{hydrolysis}/k'_{hydrolysis}$. This phenomenon resembles dynamic kinetic resolution in asymmetric catalysis, denoted dynamic kinetic hydrolysis. In the latter case, if $\Delta\Delta G^{\ddagger} > \Delta G°$, the selectivity of the ring-opening step, and as a consequence directionality, would be amplified compared with the former situation.

To ensure continuous rotation along the biaryl C–C bond in **Motor-3** when fuelled by chemical energy (Fig. 1c), all kinetic parameters are fine-tuned to ensure both cyclization and hydrolysis occur in the same reaction mixture and the molecular motor continuously rotates efficiently as long as the fuel is present. It should be emphasized that the working mechanism of the current molecular motor being kinetically driven resembles that of a second-generation light-driven molecular motor, albeit with a difference in energy input[31,40].

To confirm the crucial role of two adjacent stereocentres in the benzyl and α-position to the carboxylic group, a series of model compounds (**1**, **2**, **3** and **Motor-1**) were synthesized and the ratios of kinetic/ thermodynamic (unstable/stable or abbreviated as K/T) isomers after cyclization (step 1) and helix inversion (step 2) were determined (Supplementary Sections 2 and 3). As shown in Fig. 1d, compound **1** with a single stereocentre at the benzylic position gave a high cyclization selectivity towards the kinetic isomer (K/T > 20/1) but a poor biaryl helix inversion ratio (K/T = 1/1.6). In contrast, compound **2** with a single stereocentre at the α-position to the carboxylic acid exhibited a poor cyclization selectivity (K/T = 1/1.9) but a good biaryl inversion ratio (K/T = 1/9.5). The above results clearly indicated that the stereocentre at the benzylic position and the one at the α-position of carboxylic acid were responsible for the stereocontrol in the cyclization and biaryl
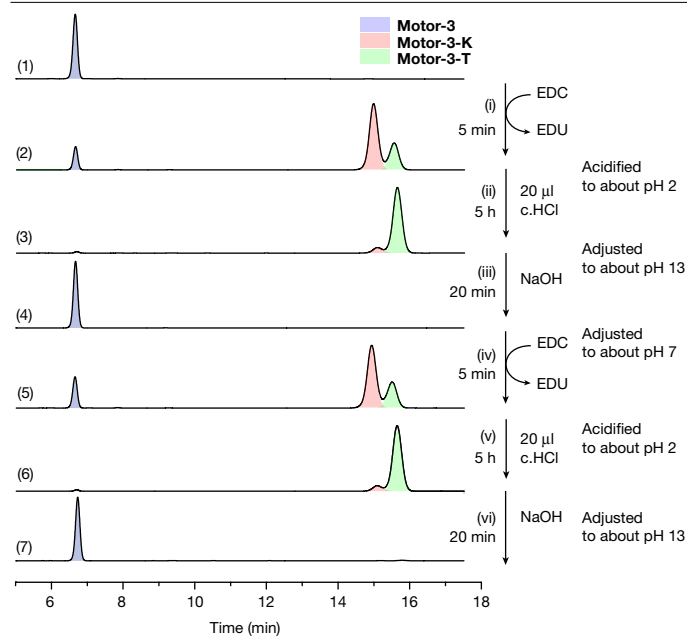
Fig. 3 | Synchronized 360° rotation with pulses of chemical fuel and acid–base oscillations. Reagents and conditions: **Motor-3** (5 mg, 0.013 mmol), DCM (2.0 ml), H_2O (3.0 ml), 25 °C (Supplementary Section 10, Agilent Pursuit XRs 5 C18 250 × 4.6 mm, 25 °C, 1.0 ml min^{-1}, MeCN/H_2O/HCOOH = 70/30/0.1, λ = 280 nm). (1) HPLC trace of the initial state of the **Motor-3**. (2) HPLC trace of the sample taken from the reaction mixture after cyclization for 5 min. (3) HPLC trace of the sample taken from the reaction mixture after inversion. (4) HPLC trace of the sample taken from the reaction mixture after hydrolysis. From (1) to (4), 180° rotation of the molecular motor has been achieved in a unidirectional manner. Then (5), (6) and (7) show the second half of the cycle to achieve full 360° unidirectional rotation. (i) EDC (40 mg, 0.21 mmol), 5 min; (ii) 20 µl concentrated HCl (c.HCl), 5 h; (iii) NaOH (80 mg, 2.0 mmol), 20 min; (iv) 75 µl c.HCl, EDC (40 mg, 0.21 mmol), 5 min; (v) 20 µl c.HCl, 5 h; (vi) NaOH (80 mg, 2.0 mmol), 20 min. λ, wavelength; EDU, 1-[3-(dimethylamino)propyl]-3-ethylurea); HCOOH, formic acid; MeCN, acetonitrile.

helix inversion, respectively. We reasoned that if two stereocentres with matched configuration were introduced, high selectivity in both the cyclization and the inversion processes might be achieved. To our delight, the *syn*-isomer (*S*,*S'*)-**Motor-1** indeed showed high cyclization selectivity (K/T > 20/1) and a good helix inversion ratio (K/T = 1/4.1). In contrast, a high ratio (K/T = 1/15) of the thermodynamic product was obtained when the *anti*-isomer (*R*,*S'*)-**3** was cyclized. Exploring the delicate balance of stereochemical elements, we found that **Motor-2** with an −OH substituent at the benzylic position instead of −OMe compared with **Motor-1** shows a marked decrease in the inversion barrier (standard free energy, $\Delta^{\ddagger}G°$ = 98.0 kJ mol^{-1}; half-life, $t_{1/2}$ = 4.7 h, 298.15 K; Supplementary Fig. 10). Further experimental details on the evaluation of the motors, that is, NMR spectra of the distinct isomers and single-crystal X-ray diffraction to establish their absolute configuration and conformational analysis, are given in Extended Data Figs. 1 and 2. To further improve the speed of the rotary molecular motor, an electron-rich and sterically more demanding *t*-Bu group was introduced to 4,4′-position of the biaryl (**Motor-3**) (ref.[41]). As a result, the Gibbs standard free energy of activation of **Motor-3** was further decreased to 94.7 kJ mol^{-1} ($t_{1/2}$ = 73 min, 298.15 K) and the helix inversion ratio was also improved to 10/1 (Supplementary Fig. 11).

To prove unequivocally that the chemically fuelled molecular motor undergoes stepwise 360° unidirectional rotation about the single bond, desymmetrization of lower ring (stator) is necessary to the distinguish isomers after each step (Fig. 2). Monobromination in the presence of chiral phosphoric acid catalyst of the stator of molecular **Motor-1** provided

Motor-Br with high stereoselectivity (diastereomeric ratio (d.r.) > 25:1) (Supplementary Sections 2 and 7)[42]. The relative configuration of corresponding methyl ester **Motor-Br-Me** was determined by single-crystal diffraction analysis (Supplementary Fig. 22). The 360° rotary cycle of the molecular motor **Motor-Br** is shown in Fig. 2, and the individual steps studied by ^{1}H NMR show all the distinct isomers during the unidirectional rotary cycle. In step 1, the lactonization of (*S*,*S'*,^{a}*R*)-**Motor-Br** (where the superscript 'a' denotes the axial chirality) in the presence of 1-(3-dimethylaminopropyl)-3-ethylcarbodiimide hydrochloride (EDC) is favoured to take place with the left hydroxyl rather than the right one on the stator. The stable isomer *trans*-**Motor-Br-T** was obtained by heating the unstable isomer *trans*-**Motor-Br-K** in deuterated chloroform (CDCl$_3$) at 65 °C for 2 h and a good inversion ratio (K/T = 1/6.3) was observed. The 180° unidirectional rotation was accomplished after hydrolysis of *trans*-**Motor-Br-K** by lithium hydroxide (LiOH) to give (*S*,*S'*,^{a}*S*)-**Motor-Br**—the atropisomer of (*S*,*S'*,^{a}*R*)-**Motor-Br**. Accordingly, the remaining half cycle can be achieved with the same sequence of steps (Fig. 2; see also Supplementary Fig. 23 for full spectra). On the basis of these data, it is clear that the present chemically fuelled molecular motor indeed undergoes stepwise 360° unidirectional rotation as the sequential interconversion with excellent stereocontrol of all six isomers can be clearly identified by ^{1}H NMR spectroscopy.

With the optimized motor design, that is, **Motor-3** and stepwise 360° unidirectional rotation established, we next sought to synchronize the stepwise operation of the molecular motor (Fig. 3). Conditions were established to ensure that all the cyclization, biaryl-inversion and hydrolysis reactions took place sequentially in the reaction mixture with **Motor-3**. Initially, when EDC (2.0 equiv.) was added to a solution of **Motor-3** in dichloromethane (DCM; 2.0 ml) and water (H_2O; 3.0 ml), >80% carboxylic acid was converted to the kinetic isomer **Motor-3-K** within 5 min. However, high-performance liquid chromatography (HPLC) analysis indicated that about 30% of the kinetic isomer was converted to the stable isomer **Motor-3-T** owing to the low barrier of helix inversion (Fig. 3, (3)). Next, the system was acidified to about pH 2 by adding 20 µl concentrated hydrochloric acid (HCl), and after 5 h, >95% of the kinetic product (**Motor-3-K**) was converted to the thermodynamic isomer **Motor-3-T**. Then, the system was adjusted to about pH 13 by adding 2 mmol sodium hydroxide (NaOH), and the hydrolysis of **Motor-3-T** was completed in 20 min to give **Motor-3** showing that unidirectional 180° rotary rotation was accomplished. The remaining half cycle was realized by operation of **Motor-3** using the same reaction sequence mentioned above. As shown in Fig. 3 (6), after six steps **Motor-3** fully restored to its initial state without any impurities observed. It is evident that **Motor-3** can be operated in a synchronized 360° rotation manner by adding pulses of EDC as a chemical fuel under acid–base oscillations.

With the unequivocal proof of chemical-driven, sequential, synchronized and unidirectional steps comprising a full 360° rotary cycle, we next established the operation of the rotary molecular motor in a continuous, autonomous and unidirectional manner. We first investigated the hydrolysis rate of stable isomer ($k_{hydrolysis}$) and the unstable isomer ($k'_{hydrolysis}$) of the cyclic states as in conditions of continuous rotation, if $k_{inversion} \gg k'_{hydrolysis} > k_{hydrolysis}$, the system follows the Curtin–Hammett principle and the unidirectionality might be compromised (Fig. 4). **Motor-1** was used to study the kinetics owing to its relatively high inversion barrier, which can avoid interconversion between the kinetic and the thermodynamic isomers during the hydrolysis process. Gratifying, the hydrolysis rate constant of the stable isomer is 47 times that of the unstable isomer (Fig. 4a and Supplementary Section 8). This means we can use this marked difference in hydrolysis rate to amplify the unidirectionality of the molecular motor according to the Curtin–Hammett principle if the kinetics follows $k_{inversion} \geq k_{hydrolysis} > k'_{hydrolysis}$. Several experiments were performed with mixture of the methoxymethyl (MOM)-protected cyclic isomers (**Motor-1-MOM-K**/**Motor-1-MOM-T** = 4:1) to confirm this dynamic kinetic hydrolysis (Fig. 4b).
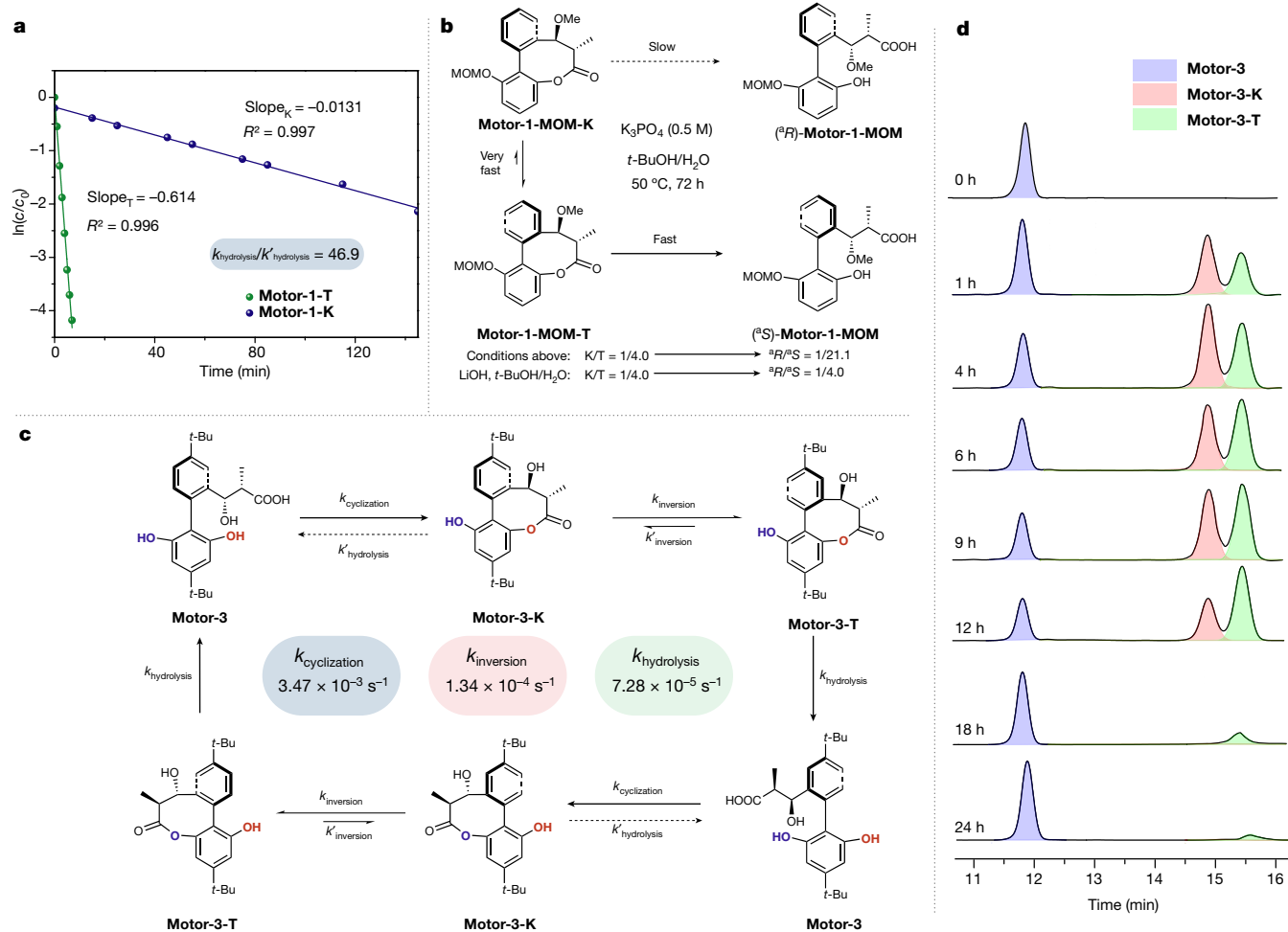
Fig. 4 | Continuous rotation of the molecular motor. a, Determination of the hydrolysis rates of **Motor-1-K** and **Motor-1-T**. **b**, Dynamic kinetic hydrolysis experiment. Reagents and conditions: **Motor-1-MOM-K** (165 mg, 0.5 mmol), 0.5 M K_3PO_4 aqueous solution (5.0 ml), *t*-BuOH (5.0 ml), 50 °C, 72 h, 88%. Control experiment: **Motor-1-MOM-K** (165 mg, 0.5 mmol), 0.5 M LiOH aqueous solution (5.0 ml), *t*-BuOH (5.0 ml), 0 °C, 10 h, 92%. **c**, The continuous rotation of the molecular motor powered by chemical fuel (Supplementary Section 15).

Reagents and conditions: **Motor-3** (20 mg, 0.05 mmol), 2 M K_3PO_4 aqueous solution (5.0 ml), *t*-BuOH (3.0 ml), 1,4-dioxane (2.0 ml), DIC (2.0 mmol), HOBt (1.0 mmol), 35 °C. **d**, HPLC chromatograms of the samples taken from the reaction mixture during the continuous rotation of the **Motor-3** from 0 h to 24 h (For analytical purposes, the carboxylic acid was converted to methyl carboxylate **Motor-3-Me**). c, concentration; c_0, initial concentration.

When the hydrolysis reaction was executed in a mixture of 0.5 M tripotassium phosphate (K_3PO_4) aqueous solution, *tert*-butanol (*t*-BuOH) at 50 °C, the d.r. of the product was indeed improved to 21/1 compared with the ratio of reactant (4:1). In contrast, when the mixture of cyclic isomers was treated with LiOH as a control experiment, the d.r. of the product was equal to the d.r. of the starting material (4/1 to 4/1) (Supplementary Fig. 28), because the hydrolysis rates are much faster than the rate of inversion ($k_{hydrolysis} > k'_{hydrolysis} \gg k_{inversion}$).

In the present system, as we have proven that the molecular motor undergoes a 360° unidirectional stepwise rotation involving 6 distinct isomers, the molecular motor should exhibit the same properties in continuous rotation mode. However, conditions should be developed to ensure both hydrolysis and cyclization can take place in the same reaction mixture allowing the molecular motor to work in an efficient way, not compromising the unidirectional rotary cycle. Two principles guide us to establish the proper condition. (1) As the rotation speed and unidirectionality of molecular motor are dependent on a set of reaction rate constants ($k_{cyclization}$, $k_{inversion}$, $k'_{hydrolysis}$ and $k_{hydrolysis}$), the values of $k_{cyclization}$ and $k_{hydrolysis}$ should be of a similar magnitude to $k_{inversion}$ to avoid that the rate-limiting step is far slower than the other steps. (2) To avoid the hydrolysis of the kinetic isomer, $k_{inversion}$ should be much larger than $k'_{hydrolysis}$ ($k_{inversion} > 100 k'_{hydrolysis}$;

Supplementary Section 12). On the basis of this analysis, we established the conditions that were compatible with both the cyclization and the hydrolysis process of **Motor-3**: 2 M aqueous K_3PO_4, *t*-BuOH and dioxane (5:3:2 v/v/v). Now the hydrolysis process can take place and meanwhile cyclization also occurs in the presence of DIC and 1-hydroxybenzotriazole (HOBt) in the same solvent mixture (Fig. 4c). With the optimized conditions for continuous rotation established, the reaction rate constant for helix inversion and the observed rate constants for cyclization and hydrolysis were determined at 35 °C ($k_{inversion} = 1.34 \times 10^{-4}$ s^{-1}, $t_{1/2} = 86.1$ min; $k_{cyclization} = 3.47 \times 10^{-3}$ s^{-1}, $t_{1/2} = 33.3$ min; $k_{hydrolysis} = 7.28 \times 10^{-5}$ s^{-1}, $t_{1/2} = 159$ min), respectively (Supplementary Sections 12–14). In the presence of excess DIC, the hydrolysis is the slowest step and the rate-determining step in the rotatory cycle. These results clearly show that the rate constants meet the criteria we indicated above (Fig. 4).

A continuous rotation experiment was performed and the process was monitored by HPLC as shown in Fig. 4d. At the starting point, DIC and HOBt were added in one batch to a solution of **Motor-3** in a mixed solvent of *t*-BuOH, dioxane and 2 M K_3PO_4 aqueous solution. Within 1 h, both cyclic isomers were detected, which can both be regarded as far-from-equilibrium states. From 4 h to 9 h, this out-of-equilibrium system reached a steady state, where the proportions of all isomers

Article

were roughly unchanged. From 9 h to 12 h, the observed cyclization rate decreased owing to the decreasing concentration of DIC, which led to the slightly decreased K/T ratio. Following the consumption of the chemical fuel (DIC) and thorough hydrolysis of cyclic isomers, this system turned back to its initial equilibrium state during 12 h to 24 h. The molecular motor will keep rotating if the amount of fuel is in excess to the motor. Finally, the hydrolysis rate of DIC (background reaction of fuel) was also determined ($k_{decomposition} = 5.64 \times 10^{-5}\,s^{-1}$, $t_{1/2} = 204$ min; Supplementary Section 11), which is much lower compared with $k_{cyclization}$ ($3.47 \times 10^{-3}\,s^{-1}$). This means the molecular motor is a good catalyst for decomposition of the fuel and, based on the rates, we can establish that 98% DIC is consumed in the early stages and the ratio drops as the concentration of the free acid form of **Motor-3** decreased. Over the 360° autonomous unidirectional rotation, the unidirectionality is determined by the kinetics of three sets of highly selective cyclization, helix inversion and hydrolysis reactions, so the unidirectionality can be calculated as: $(k_{hydrolysis}/k'_{hydrolysis})^2 \times (k_{inversion}/k'_{inversion})^2 \times (k_{cyclization}/k'_{cyclization})^2 = 47^2 \times 9^2 \times 20^2 = 7.2 \times 10^7/1$, where $k_{cyclization}/k'_{cyclization}$ is the ratio of K/T after cyclization and $k_{inversion}/k'_{inversion}$ is the ratio of T/K after helix inversion.

In conclusion, we have developed an autonomous unidirectional rotary molecular motor fuelled by chemical energy, taking advantage of intrinsic chiral elements in a system that is mainly governed by kinetics distinct from the systems operating through a small bias to mainly Brownian motion. Although still far from the rotary speeds of our light-powered motors operating in the nanosecond regime, we expect that the design principles shown here will be compatible with several other chemical transformations and fuels and probably facilitate the development of chemical powered rotary motors for a wide range of machine-like functions.

Online content

Any methods, additional references, Nature Research reporting summaries, source data, extended data, supplementary information, acknowledgements, peer review information; details of author contributions and competing interests; and statements of data and code availability are available at https://doi.org/10.1038/s41586-022-05033-0.

1. Saper, G. & Hess, H. Synthetic systems powered by biological molecular motors. *Chem. Rev.* **120**, 288–309 (2020).
2. Sowa, Y. et al. Direct observation of steps in rotation of the bacterial flagellar motor. *Nature* **437**, 916–919 (2005).
3. Boyer, P. D. The ATP synthase—a splendid molecular machine. *Annu. Rev. Biochem.* **66**, 717–749 (1997).
4. Wang, J. & Feringa, B. L. Dynamic control of chiral space in a catalytic asymmetric reaction using a molecular motor. *Science* **331**, 1429–1432 (2011).
5. Roke, D., Wezenberg, S. J. & Feringa, B. L. Molecular rotary motors: unidirectional motion around double bonds. *Proc. Natl Acad. Sci. USA* **115**, 9423–9431 (2018).
6. Browne, W. R. & Feringa, B. L. Making molecular machines work. *Nat. Nanotechnol.* **1**, 25–35 (2006).
7. Kelly, T. R. et al. Progress toward a rationally designed, chemically powered rotary molecular motor. *J. Am. Chem. Soc.* **129**, 376–386 (2007).
8. Anelli, P. L., Spencer, N. & Stoddart, J. F. A molecular shuttle. *J. Am. Chem. Soc.* **113**, 5131–5133 (1991).
9. Badjić, J. D., Balzani, V., Credi, A., Silvi, S. & Stoddart, J. F. A molecular elevator. *Science* **303**, 1845–1849 (2004).
10. Cárdenas, D. J., Livoreil, A. & Sauvage, J.-P. Redox control of the ring-gliding motion in a Cu-complexed catenane: a process involving three distinct geometries. *J. Am. Chem. Soc.* **118**, 11980–11981 (1996).
11. Jiménez, M. C., Dietrich-Buchecker, C. & Sauvage, J.-P. Towards synthetic molecular muscles: contraction and stretching of a linear rotaxane dimer. *Angew. Chem. Int. Ed.* **39**, 3284–3287 (2000).
12. Silvi, S., Venturi, M. & Credi, A. Artificial molecular shuttles: from concepts to devices. *J. Mater. Chem.* **19**, 2279–2294 (2009).
13. Stevens, A. M. & Richards, C. J. A metallocene molecular gear. *Tetrahedron Lett.* **38**, 7805–7808 (1997).
14. Geeves, M. A. & Holmes, K. C. Structural mechanism of muscle contraction. *Annu. Rev. Biophys.* **68**, 687–728 (1999).
15. Hua, W., Chung, J. & Gelles, J. Distinguishing inchworm and hand-over-hand processive kinesin movement by neck rotation measurements. *Science* **295**, 844–848 (2002).
16. Vale, R. D. The molecular motor toolbox for intracellular transport. *Cell* **112**, 467–480 (2003).
17. Erbas-Cakmak, S., Leigh, D. A., McTernan, C. T. & Nussbaumer, A. L. Artificial molecular machines. *Chem. Rev.* **115**, 10081–10206 (2015).
18. van Dijk, L. et al. Molecular machines for catalysis. *Nat. Rev. Chem.* **2**, 0117 (2018).
19. Aprahamian, I. The future of molecular machines. *ACS Cent. Sci.* **6**, 347–358 (2020).
20. Astumian, R. D. Kinetic asymmetry allows macromolecular catalysts to drive an information ratchet. *Nat. Commun.* **10**, 3837 (2019).
21. Koumura, N., Zijlstra, R. W. J., van Delden, R. A., Harada, N. & Feringa, B. L. Light-driven monodirectional molecular rotor. *Nature* **401**, 152–155 (1999).
22. Kelly, T. R., De Silva, H. & Silva, R. A. Unidirectional rotary motion in a molecular system. *Nature* **401**, 150–152 (1999).
23. Greb, L. & Lehn, J.-M. Light-driven molecular motors: imines as four-step or two-step unidirectional rotors. *J. Am. Chem. Soc.* **136**, 13114–13117 (2014).
24. Erbas-Cakmak, S. et al. Rotary and linear molecular motors driven by pulses of a chemical fuel. *Science* **358**, 340–343 (2017).
25. Bach, N. N., Josef, V., Maid, H. & Dube, H. Active mechanical threading by a molecular motor. *Angew. Chem. Int. Ed.* **61**, e202201882 (2022).
26. Fletcher, S. P., Dumur, F., Pollard, M. M. & Feringa, B. L. A reversible, unidirectional molecular rotary motor driven by chemical energy. *Science* **310**, 80–82 (2005).
27. Collins, B. S. L., Kistemaker, J. C. M., Otten, E. & Feringa, B. L. A chemically powered unidirectional rotary molecular motor based on a palladium redox cycle. *Nat. Chem.* **8**, 860–866 (2016).
28. Zhang, Y. et al. A chemically driven rotary molecular motor based on reversible lactone formation with perfect unidirectionality. *Chem* **6**, 2420–2429 (2020).
29. Corra, S. et al. Artificial supramolecular pumps powered by light. *Chem. Eur. J.* **27**, 11076–11083 (2021).
30. Guentner, M. et al. Sunlight-powered kHz rotation of a hemithioindigo-based molecular motor. *Nat. Commun.* **6**, 8406 (2015).
31. Koumura, N., Geertsema, E. M., van Gelder, M. B., Meetsma, A. & Feringa, B. L. Second generation light-driven molecular motors. Unidirectional rotation controlled by a single stereogenic center with near-perfect photoequilibria and acceleration of the speed of rotation by structural modification. *J. Am. Chem. Soc.* **124**, 5037–5051 (2002).
32. Lubbe, A. S. et al. Photoswitching of DNA hybridization using a molecular motor. *J. Am. Chem. Soc.* **140**, 5069–5076 (2018).
33. Pooler, D. R. S., Lubbe, A. S., Crespi, S. & Feringa, B. L. Designing light-driven rotary molecular motors. *Chem. Sci.* **12**, 14964–14986 (2021).
34. Štacko, P. et al. Locked synchronous rotor motion in a molecular motor. *Science* **356**, 964–968 (2017).
35. Zhao, D., van Leeuwen, T., Cheng, J. & Feringa, B. L. Dynamic control of chirality and self-assembly of double-stranded helicates with light. *Nat. Chem.* **9**, 250–256 (2016).
36. Wilson, M. R. et al. An autonomous chemically fuelled small-molecule motor. *Nature* **534**, 235–240 (2016).
37. Borsley, S., Kreidt, E., Leigh, D. A. & Roberts, B. M. W. Autonomous fuelled directional rotation about a covalent single bond. *Nature* **604**, 80–85 (2022).
38. Bringmann, G. et al. Atroposelective synthesis of axially chiral biaryl compounds. *Angew. Chem. Int. Ed.* **44**, 5384–5427 (2005).
39. Seeman, J. I. The Curtin–Hammett principle and the Winstein–Holness equation: new definition and recent extensions to classical concepts. *J. Chem. Educ.* **63**, 42–48 (1986).
40. Koumura, N., Geertsema, E. M., Meetsma, A. & Feringa, B. L. Light-driven molecular rotor: unidirectional rotation controlled by a single stereogenic center. *J. Am. Chem. Soc.* **122**, 12005–12006 (2000).
41. Aikawa, K., Miyazaki, Y. & Mikami, K. Stable axial chirality in metal complexes bearing 4,4'-substituted BIPHEPs: application to catalytic asymmetric carbon–carbon bond-forming reactions. *Bull. Chem. Soc. Jpn* **85**, 201–208 (2012).
42. Mori, K. et al. Enantioselective synthesis of multisubstituted biaryl skeleton by chiral phosphoric acid catalyzed desymmetrization/kinetic resolution sequence. *J. Am. Chem. Soc.* **135**, 3964–3970 (2013).

a

direction of cyclization

(*S*,*S'*)-**Motor-1-Me**
Syn-configuration

(*R*,*S'*)-**3-Me**
Anti-configuration

b

eq

ax

Motor-1-K
Front view

Motor-1-K
Top view

ax

eq

Motor-1-T-MOM
Front view

Motor-1-T-MOM
Top view

Extended Data Fig. 1 | Single-crystal structures of 3-Me, Motor-1-Me, Motor-1-K and MOM-derived thermodynamic product (Motor-1-T-MOM). (a) The absolute configuration of molecular motors was unambiguously established by single-crystal X-ray diffraction as well (Here, the *S* or *R* denotes the configuration of the chiral centre at the α position of carboxylic acid group, *S'* or *R'* denotes the configuration of the chiral centre of the benzyl position). Single crystal X-ray diffraction experiments of the corresponding methyl esters **3-Me** and **Motor-1-Me** were performed to gain insight into the relationship between configurations and cyclization selectivity. The results indicated the orientation of the carboxylic group is key to realize high selectivity of cyclization. Viewed along the biaryl C–C bond (the axle of rotation), the carboxylic group in (*S*,*S'*)-*syn*-isomer–**1** favours bridge formation with the hydroxyl group on the right of the stator aryl to generate exclusively the kinetic isomer. However, the methyl group at the α-position of the carboxylic group in (*R*,*S'*)-*anti*-isomer **3** blocked the carboxylic group from reacting with hydroxyl group on the right side of the stator aryl and therefore cyclized with the left hydroxyl group to give dominantly a thermodynamic isomer. (b) Single-crystal X-Ray diffraction of **Motor-1-K** and MOM-protected **Motor-1-T-MOM** confirmed that the rotational direction of **Motor-1** was clockwise. It is interesting to note the favoured tub-shaped conformation of the eight-membered ring in **Motor-1-T** and **Motor-1-K**. In **Motor-1-K**, the methyl group adopts a pseudoaxial orientation while the methoxy group is located in a pseudoequatorial position. However, in the case of **Motor-1-T**, the methoxy group is in a pseudoaxial orientation and the methyl group adopts a pseudoequatorial position. The eight-membered ring flipping can be explained by Winstein–Holness A value which is used to describe the conformational preference of an equatorial compared to an axial substituent in a substituted cyclohexane. As the A value of a methyl group (1.7 kcal/mol) is larger than the A value of a methoxy group (0.6 kcal/mol), the methyl group has a strong tendency for the equatorial position which also drives the helix inversion of the biaryl and the conversion of **Motor-1-K** to **Motor-1-T** (*P* to *M*).
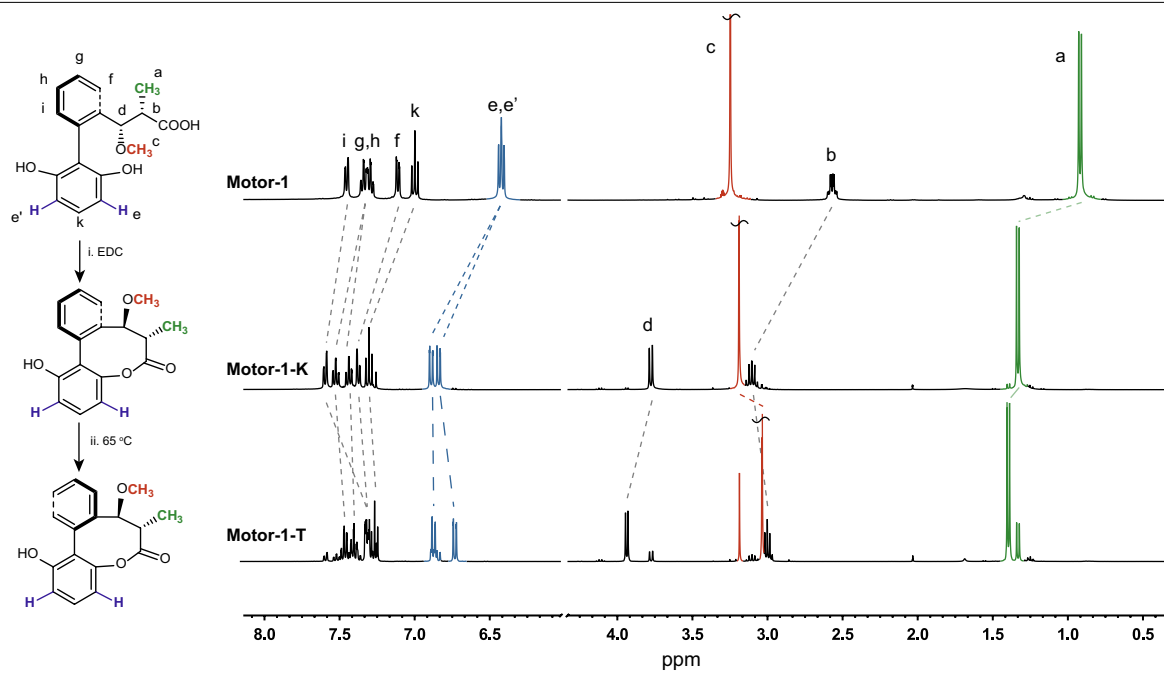
Extended Data Fig. 2 | ¹H NMR spectra of three stations of Motor-1. ¹H NMR spectra of three states (**Motor-1, Motor-1-K, Motor-1-T**) during the 180° unidirectional rotation. In the first step, **Motor-1** was cyclized to give a high-energy isomer **Motor-1-K** in the presence of the fuel EDC in DCM at 0 °C and this is the only energy input step in the half cycle of rotation. **Motor-1-K** unstable isomer then underwent an energetic downhill helix inversion to yield the **Motor-1-T** with a final ratio of T/K = 4/1. Analysis of the kinetic data provided the Gibbs free energy of activation $\Delta^{\ddagger}G° = 103.6$ kJ/mol ($t_{1/2} = 45$ h at 298.15 K) (Supplementary Fig. 9).